


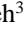






Simulation and Analysis of the SnSe/Au Nanolayer Using SPR Technique for Biosensing Applications

Farah A. Jasim^{1*}, Farah J. Kadhum¹, Marwah N. Merza², Anwar H. Al-Saleh³, Ali A. Al-Zuky¹,
Nabeel M. Mirza⁴

¹ Department of Physics, College of Science, Mustansiriyah University, Baghdad 10052, Iraq

² Department of Information Technology, College of Computer and Information Technology, University of Garmian, Kurdistan Region 32007, Iraq

³ Department of Computer, College of Science, Mustansiriyah University, Baghdad 10052, Iraq

⁴ Department of Physics, College of Education, Mustansiriyah University, Baghdad 10052, Iraq

Corresponding Author Email: Farah.A.J@uomustansiriyah.edu.iq

Copyright: ©2024 The authors. This article is published by IETA and is licensed under the CC BY 4.0 license (<http://creativecommons.org/licenses/by/4.0/>).

<https://doi.org/10.18280/i2m.230508>

ABSTRACT

Received: 22 January 2024

Revised: 5 August 2024

Accepted: 13 September 2024

Available online: 25 October 2024

Keywords:

tin selenide, biosensor, otto configuration, TMM, sensitivity, FWHM

Surface plasmons (SPs) originate at the interface, or the boundaries between the metal and dielectric material, when p-polarized light in an electric or magnetic field excites electrons on the surface of a conducting material, causing electronic oscillations on the surface of metal or material. Surface plasmon resonance (SPR) is a very promising optical method that is being employed in various structures to detect substances for chemical, environmental, biological, and medicinal purposes. Furthermore, one of the best sensors for biomolecular sample identification is SPR-based technology because of its high sensitivity and rapid response. Gold and silver are the most commonly used metals due to their strong sensitivity for SPR biosensors in the visible and near-infrared bands. Therefore, the high sensitivity of gold is the most important feature to exploit when designing a surface plasmon resonance (SPR) sensor in an effort to increase sensor reliability. The motivation for this research is to work on developing biosensors with high accuracy and improved sensitivity for the detection of various biological molecules, which contributes to advances in the fields of medical diagnosis and healthcare. This work deals with the Otto configuration with two layers covering the N-LASF9 hemi-cylindrical prism. Tin selenide (SnSe), which is 10-80 nm thick, forms the first layer, and gold (Au), which is 50 nm thick, forms the second layer. The article centered around discovering the effective regions of the electromagnetic spectrum of the designed SPR biosensor based on the reflectivity curve (RC). RC measurements involve quality factor (QF), detection accuracy (DA), and sensitivity (S). The transfer matrix method (TMM) was used to implement and select simulation tools such as optical and geometrical parameters for both tin selenide and gold nanolayers. The parameters include thickness, incident light wavelength, refractive indices, etc. The sensing performance parameters FWHM, SPR dip (L_d), DA, and QF were investigated. According to the numerical results obtained, the sensitivity of the designed sensor reached 100 degrees/RIU, and it has a high detection accuracy when compared to other biosensors. The designed biosensor was also shown to be suitable for detecting in the visible and near-infrared ranges.

1. INTRODUCTION

Surface plasmons (SPs) are formed when an electric or magnetic field of p-polarized light excites electrons on a conducting material's surface, causing electronic oscillations to the surface of the material or metal. Stated differently, they originate at the boundaries of the dielectric materials and metals (the interface). SPs are thought of as electromagnetic waves because of the way these interactions happen at the interface between dielectric and metal [1]. The excited electrons have a high density and are known as plasmons because they display harmonic oscillations near the contact. The metal may produce potent SPs when it is positioned as a

layer on the prism and comes into contact with the dielectric [2]. The well-known applications of SPR biosensors include sensing gases, studying surface interactions, and biomaterial detection [3].

Recently, an SPR-based optical biosensor technique has been developed with free-label and real-time detection capability [4]. In most of the SPR investigations, both silver and gold are the most commonly used metals due to their strong sensitivity for SPR biosensors in the visible and near-infrared bands [3]. Conventional SPR sensor systems make use of the gold or silver deposited on a massive prism as well as an optical process called incident light stimulation at the metal-dielectric interface [5]. Then, the light reflected from the

thin metal prism is measured using SPR sensors for both incidence angle and light intensity [5]. The rapid expansion of SPR-based biosensors across a broad range of applications has led to a number of researchers conducting a variety of investigations to date. These methods are being used more often in military and defense [6], environmental monitoring [7], agriculture [8], food and water quality control [9], medical diagnostics [10], and ultra-sensitive and quick biological material detection fields [11, 12]. Our work contributes to the analysis and knowledge of how the tin selenide layer affects the conceptual model and structural design of the proposed SPR sensor. The sensor performance is determined using the reflectivity curves of the SnSe/Au nanolayers.

Since the invention of the first SPR sensor by Nylander et al. [13] in 1982 for biosensing and gas sensing, many researchers have devised a variety of methods to increase the sensitivity of SPR. Each strategy has its own unique design among a wide range of elements in SPR design, such as Bragg grating-based SPR, supercontinuum exciting SPR, optical design, magneto-optic SPR, plasmonic materials, Fabry-Perot-based SPR, and nanomaterials. In addition, the sensitivity of SPR considerably changes depending on the kind of dielectric, such as gas or liquid, as well as the type of structure, such as a diffraction grating, a prism, or an optical fiber.

Tin selenide is a P-type semiconductor material that is both chemically resistant and non-toxic. It features a gap of 0.9 eV for indirect transitions and a gap of 1.3 eV for direct transitions. It is a distinctive, multilayer-structured plasmonic material with excellent electrical and optical characteristics that attracts much interest as a two-dimensional substrate. Films manufactured from SnSe have a high transmittance (56-76%) and a high refractive index (2.05-2.55), so they are suitable for applications in photovoltaics, optical fibers, solar cells, etc. Therefore, many researchers have implemented different approaches with SnSe in different experiments. In 2019, Dai et al. [14] improved the sensitivity of the sensor while maintaining its chemical stability by adding three different types of 2-D SnSe to the structure between the metallic silver (Ag) thin and the sensing medium. Their goal was achieved, as they found that adding SnSe allotropes to the silver films enhanced the sensitivity. In another experiment in 2022, Dwivedi et al. [15] presented a configuration for a surface plasmon resonance (SPR) sensor to detect anemia, abnormalities in urine, and DNA hybridization. The configuration consisted of zinc oxide (ZnO) and tin di-selenide (SnSe₂) as the stacked structure on the prism (SF-10).

In an investigation by Varasteanu [16], 2019, he deposited an allotrope of SnSe (α , δ , and ϵ) monolayer on a gold layer for improving the interaction of SPR sensors and increasing their reflectivity and phase sensitivity. They did not address the practical constraints, scalability of the manufacturing process, or potential roadblocks in converting the simulation-based SnSe/gold-based SPR sensor into a feasible one in their proposal. In order to guarantee the robustness and dependability of the designed instrument when applied to practical scenarios, it is important to keep in mind that the success of these kinds of sensors frequently depends on structural parameters like the wavelength used, the type of prism, the refractive index of the sensing medium, the angles of incidence of the light source, and others. In 2023, Mohamad et al. [17], simulated a surface plasmon resonance (SPR) sensor for a gas sensor. They deposited a silver/cadmium sulfide (Ag/CdS) based on the Kretschmann configuration. They analyzed their results based on the reflectivity curves and

used (detection accuracy, quality factor, sensitivity, and FWHM) as parameters to determine the sensor's performance. The authors investigated the effects of various design parameters, such as the wavelength of the light source and the thickness of the CdS and Ag layers, on the sensor's performance in order to make well-informed design decisions. In contrast, the experiment in this study employed the Otto configuration to build and test a biosensor system using a conductive material (Au) with a thickness of 50 nm placed over an insulating material (SnSe) with a variable thickness of 0-80 nm.

Recently, a paper [18] was published that deals with the simulation of a SPR sensor for a gas sensing. They used the Kretschmann setup to deposit tantalum pentoxide on silver (Ag/Ta₂O₅). The Ta₂O₅ layer's thickness varied from 0 to 70 nm, whereas the silver layer's thickness was constant at 50 nm. Their study is similar to our research with respect to simulation boundary conditions, sensor performance metrics, and prism glass type. Nevertheless, they left out of their proposal any discussion of the manufacturing process's scalability, practical constraints, or potential obstacles to turning the Ag/Ta₂O₅-based SPR sensor model into a workable sensor.

The starting point of our study is to provide new theoretical analyses that have not yet been applied in practice but represent a fundamental step that can be used in future practical applications to improve the accuracy and sensitivity of biosensors through studying the simulation and configuration of a nanolayer of SnSe/Au using SPR technology for biosensing purposes.

This work aims to investigate the SnSe/Au sensor's sensitivity through the transfer matrix method (TMM) [19]. The sensitivity is determined by calculating the reflectance of multilayer structures. Since many performance improvement studies for this type of sensor have relied on computational methodologies like genetic algorithms [19-21] or particle swarm optimization [22-24], they are usually complex and time-consuming to configure. As a result, we used the TMM framework methodology to obtain simulation results for varying the SnSe layer thickness.

2. THEORETICAL MODELING OF SPR BIOSENSOR

SPR-based sensors need to work well since they are utilized to find very small differences, like the refractive index of the sensing medium. Therefore, we simulate the metal/dielectric interface biosensor operating in the 300-1000 nm wavelength range and compute the electromagnetic wave reflectivity for these interface layers. The Otto configuration, depicted in Figure 1, serves as the foundation for the proposed two-layer SPR biosensor construction, which is constructed in accordance with the concept of attenuation total reflection (ATR). This work adds to the understanding of how the tin selenide layer affects the design structure and conceptual model.

The simulation details for the study include changing the SnSe layer thickness from 0 to 80 nm by an increment of 10 each time, as well as the wavelength from 300 to 1000 nm. Variable refractive indices were chosen in accordance with the wavelengths of each material, and the incident beam's angle of incidence was adjusted between 0° and 90°. Regarding the external sensing media, the value of Δn was thought to indicate the degree of contamination existing in the medium; that is, if the value is zero, the medium is pure, and if it is (0.01), the

medium is polluted, meaning that the refractive index of the medium has been altered by contamination. The subsequent paragraphs of the paper provide a detailed explanation of these factors.

The occurrence of the plasmonic resonance property depends mainly on structural parameters such as the wavelength used, the refractive index of the sensing medium, the angles of incidence of the light source, etc., and not on the properties of the materials. Other properties, such as dielectric constants and loss factors of SnSe and Au, are not important in the operation of the proposed design and do not affect it.

The Otto structure of the designed SPR biosensor is shown in Figure 1. It consists of two layers covering an N-LASF9 glass (hemi-cylindrical prism), one of which is a tin selenide (SnSe) layer with a thickness that ranges from 10 to 80 nm, and the other of which is a 50 nm layer of gold (Au).

In our simulation, the refractive index of the sensing medium was assumed to be $n_s=1.330+\Delta n_s$, where Δn_s is the variation of RI for the sensing medium, which was set at 0 and 0.01. The operational wavelength for the proposed biosensor design ranged from 300 to 1000 nm.

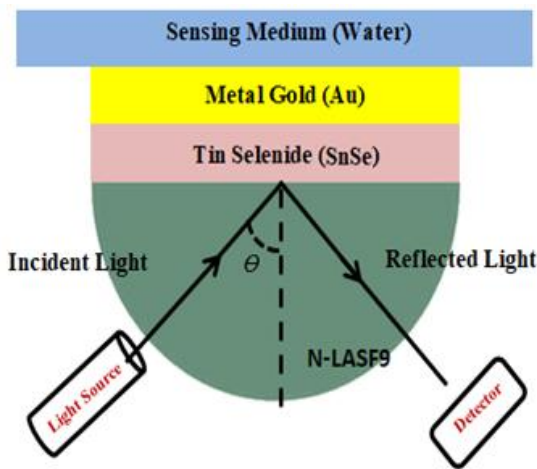


Figure 1. Representation diagram of the proposed SPR biosensor (N-LASF9/SnSe/Au)

3. REFLECTIVITY OF MULTILAYER STRUCTURE

To verify the functionality of an SPR sensor, an accurate measurement of the intensity of the reflected light at the output terminal is required. In this work, a transfer matrix has been used to develop Matlab simulation software for a system that consists of two deposited layers on a hemi-cylindrical prism: a fixed layer of gold with a thickness of 50 nm and a variable layer of tin selenide with a thickness of 10-80 nm. The following boundary conditions and Fresnel equations for the reflection of electromagnetic waves in the visible range and near infrared were selected by the simulation program [14, 25]:

$$\begin{bmatrix} E_1 \\ B_1 \end{bmatrix} = \Omega \begin{bmatrix} E_{N-1} \\ B_{N-1} \end{bmatrix} \quad (1)$$

where, B_j and E_j represent the tangential magnetic and electrical field components in the first layer of the boundary. The tangential elements of the electric and magnetic fields at the last layer are designated E_{N-1} and B_{N-1} . The characteristics matrix of the composite design, called Ω , contains P_{ij} elements and is obtained by [14, 25]:

$$\Omega = \prod_{k=2}^{N-1} P_k \begin{bmatrix} P_{11} & P_{12} \\ P_{21} & P_{22} \end{bmatrix} \quad (2)$$

with

$$P_k = \begin{bmatrix} \cos \beta_k & \frac{-i}{q_k} \sin \beta_k \\ -i q_k \sin \beta_k & \cos \beta_k \end{bmatrix} \quad (3)$$

where, β_k is phase thickness, k is a random number, and is represented by [25]:

$$\beta_k = \frac{2\pi}{\lambda} (d_k) \sqrt{(\epsilon_k - n^2 \sin^2 \theta_o)} \quad (4)$$

λ is wavelength of the incident light; ϵ_k represent the dielectric constant; θ_o is the angle of incidence; n indicates the refractive index of the glass prism; q_k stands for the refractive index of the equivalent layers and is denoted by:

$$q_k = \sqrt{(\epsilon_k - n^2 \sin^2 \theta_o)} / \epsilon_k \quad (5)$$

The reflection coefficient (r_p) for incident polarized light is written as [25]:

$$r_p = \frac{(P_{11} + P_{12} q_N) q_1 - (P_{21} + P_{22} q_N)}{(P_{11} + P_{12} q_N) q_1 + (P_{21} + P_{22} q_N)} \quad (6)$$

The following formula [26] is used to ultimately determine the reflectivity of the multi-layer structure:

$$R_p = |r_p|^2 \quad (7)$$

4. PERFORMANCE MEASUREMENTS OF THE SPR SENSOR

Performance measurements used to assess sensor quality include full-width half maximum (FWHM), sensitivity (S), quality factor (QF), and detection accuracy (DA). All of the aforementioned parameters must be increased as much as possible to enhance the function of the SPR sensor [27].

4.1 Detection accuracy (DA)

The detection accuracy (DA), sometimes called the signal to noise ratio (S/N) or abbreviated as SNR, describes the relationship between the change in resonance angle ($\Delta\theta_{RES}$) and full-width half maximum (FWHM) of the reflectance curve [28], which is expressed as follows:

$$DA = \frac{\Delta\theta_{RES}}{FWHM} \quad (8)$$

4.2 Sensitivity (S)

The idea of sensitivity of an SPR-based sensor can be defined as the variation in refractive indices (Δn_s) that causes a change in resonance angle ($\Delta\theta_{RES}$). The sensitivity is measured at degree/RIU, which may be represented mathematically as follows [29]:

$$S = \frac{\Delta\theta_{RES}}{\Delta n_s} \quad (9)$$

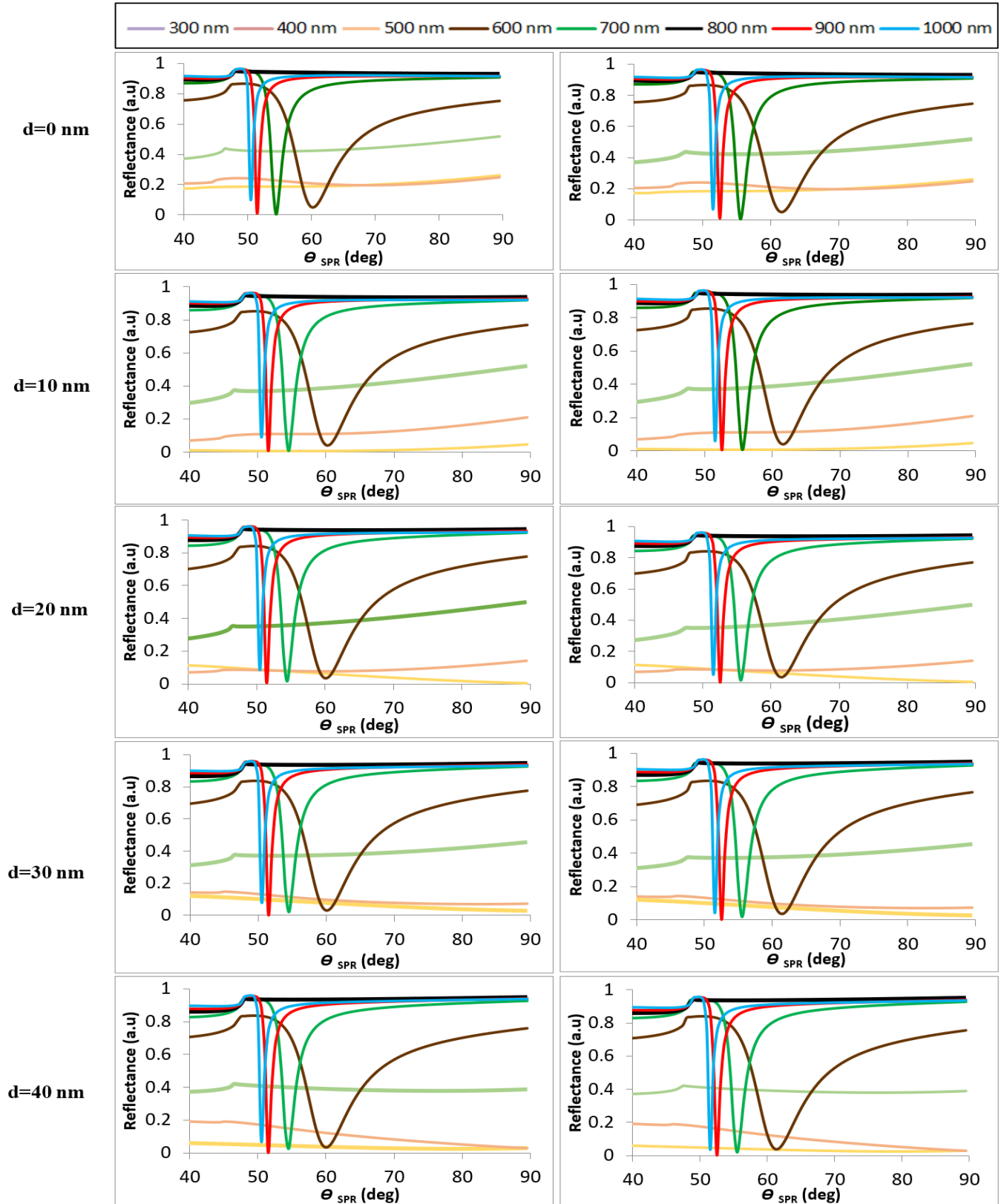
4.3 Quality factor (QF)

The quality factor (QF), sometimes called the figure of merit or abbreviated as (FOM), is defined as the relationship of the full-width half maximum (FWHM) of the reflectance curve with the sensitivity (S) of the sensor. It is measured at 1/RIU and expressed as follows [30]:

$$QF = \frac{S}{FWHM} \quad (10)$$

5. RESULTS AND DISCUSSIONS

The Otto configuration of the SnSe/Au metal has contributed to simulating the refractive index biosensor characteristic in the suggested innovative structure. The proposed refractive index sensor showed high sensitivity, making it suitable for a variety of applications, including the detection of biological fluids dissolving in water, hard water detection, and biochemistry combined with water molecules.



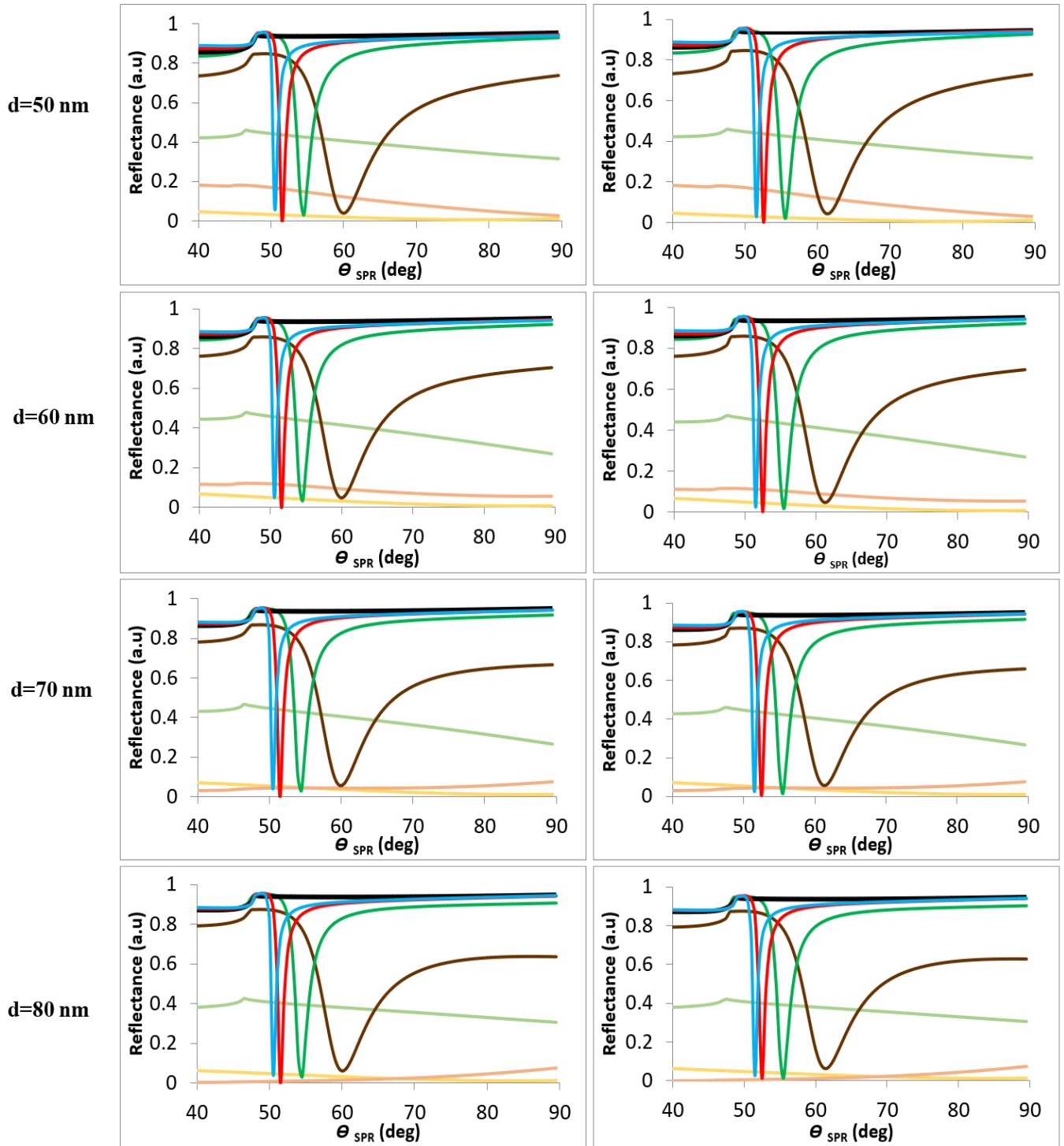


Figure 2. The reflectance curve as a function of light incidence angle for the SnSe nanolayer on Au with varying thicknesses (0-80) nm and different RI: left ($n=1.33$), right ($n=1.34$)

Table 1. The performance parameters of the biosensor at 600 nm wavelength

Thickness (nm)	$\Delta n=0$					$\Delta n=0.01$					
	Θ_{SPR} (deg)	FWHM (deg)	L_d (deg)	D.A.	Q.F. (1/RIU)	Θ_{SPR} (deg)	FWHM (deg)	L_d (deg)	D.A.	Q.F. (1/RIU)	S (deg/RIU)
0	60.2	9.2	0.8	0.15	15.2	61.6	9.5	0.81	0.14	14.7	140
10	60.2	9	0.8	0.15	14.4	61.5	9.3	0.81	0.15	13.9	130
20	60.2	9	0.8	0.15	14.4	61.5	9.3	0.8	0.15	13.9	130
30	60.1	9	0.8	0.15	14.4	61.4	9.3	0.8	0.15	13.9	130
40	60	9	0.8	0.15	15.5	61.4	9.4	0.8	0.14	14.8	140
50	60	9.1	0.8	0.15	14.2	61.3	9.5	0.8	0.14	13.6	130
60	60	9.2	0.8	0.15	14.1	61.3	9.7	0.81	0.14	13.4	130
70	60	9.3	0.8	0.15	15.0	61.4	9.9	0.81	0.14	14.1	140
80	60	9.5	0.8	0.14	14.7	61.4	10.1	0.81	0.13	13.8	140

Table 2. The performance parameters of the biosensor at 700 nm wavelength

Thickness (nm)	$\Delta n=0$					$\Delta n=0.01$					
	Θ_{SPR} (deg)	FWHM (deg)	L_d (deg)	D.A.	Q.F. (1/RIU)	Θ_{SPR} (deg)	FWHM (deg)	L_d (deg)	D.A.	Q.F. (1/RIU)	S (deg/RIU)
0	54.5	2.2	0.94	0.45	50	55.6	2.2	0.95	0.45	50	110
10	54.5	2.2	0.94	0.45	50	55.6	2.3	0.94	0.43	47.8	110
20	54.5	2.3	0.93	0.43	47.8	55.6	2.4	0.93	0.41	45.8	110
30	54.5	2.3	0.94	0.43	43.4	55.5	2.4	0.92	0.41	41.6	100
40	54.4	2.3	0.91	0.43	47.8	55.5	2.4	0.92	0.41	45.8	110
50	54.4	2.3	0.91	0.43	47.8	55.5	2.3	0.92	0.43	47.8	110
60	54.4	2.2	0.92	0.45	50	55.5	2.3	0.92	0.43	47.8	110
70	54.4	2.2	0.92	0.45	45.4	55.4	2.3	0.93	0.43	43.4	100
80	54.4	2.1	0.93	0.47	47.6	55.4	2.1	0.93	0.47	47.6	100

Table 3. The performance parameters of the biosensor at 900 nm wavelength

Thickness (nm)	$\Delta n=0$					$\Delta n=0.01$					
	Θ_{SPR} (deg)	FWHM (deg)	L_d (deg)	D.A.	Q.F. (1/RIU)	Θ_{SPR} (deg)	FWHM (deg)	L_d (deg)	D.A.	Q.F. (1/RIU)	S (deg/RIU)
0	51.5	0.8	0.95	1.25	125	52.5	0.9	0.95	1.11	111	100
10	51.5	0.8	0.95	1.25	125	52.5	0.9	0.95	1.11	111	100
20	51.5	0.9	0.95	1.11	111	52.5	0.9	0.95	1.11	111	100
30	51.5	0.9	0.95	1.11	111	52.5	0.9	0.95	1.11	111	100
40	51.5	0.9	0.95	1.11	111	52.5	0.9	0.95	1.11	111	100
50	51.5	1	0.95	1.00	100	52.5	0.9	0.92	1.11	111	100
60	51.5	1.4	0.92	0.71	71.4	52.5	1.5	0.95	0.66	66	100
70	51.5	0.9	0.95	1.11	111	52.5	0.9	0.95	1.11	111	100
80	51.5	0.9	0.95	1.11	111	52.5	0.9	0.94	1.11	111	100

Table 4. The performance parameters of the biosensor at 1000 nm wavelength

Thickness (nm)	$\Delta n=0$					$\Delta n=0.01$					
	Θ_{SPR} (deg)	FWHM (deg)	L_d (deg)	D.A.	Q.F. (1/RIU)	Θ_{SPR} (deg)	FWHM (deg)	L_d (deg)	D.A.	Q.F. (1/RIU)	S (deg/RIU)
0	50.5	0.7	0.88	1.42	143	51.5	0.7	0.89	1.42	142	100
10	50.5	0.8	0.89	1.25	125	51.5	0.7	0.91	1.43	143	100
20	50.6	0.8	0.89	1.25	113	51.5	0.7	0.91	1.43	128	90
30	50.6	0.9	0.89	1.11	100	51.5	0.9	0.92	1.11	100	90
40	50.6	0.9	0.9	1.11	100	51.5	0.9	0.92	1.11	100	90
50	50.6	1	0.9	1	90	51.5	0.9	0.92	1.11	100	90
60	50.6	0.8	0.91	1.25	113	51.5	0.7	0.92	1.43	128	90
70	50.5	0.9	0.92	1.11	111	51.5	0.9	0.92	1.11	111	100
80	50.5	0.8	0.92	1.25	125	51.5	0.7	0.93	1.43	143	100

In order to accurately determine the sensitivity capability of the SPR sensor, the reflectance curve was examined as a function of the incident angle. Different thicknesses of the SnSe layers (0, 10,..., 80 nm) were analyzed, and then the simulation results were used to determine the maximal sensitivity of the designed SPR model. In the designed sensor, it was assumed that the RI of the sensing medium changes from 1.33 to 1.34 and that the thickness of Au is 50 nm.

This paper deals with simulation to find the optimal regions where plasmonic resonance occurs, which has not been achieved in earlier research using this model. Our study attempts to give an appropriate design and numerical values for the parameters that might help to improve the practical performance of biological sensors, whereas prior studies concentrated on various materials and approaches. This analysis will provide clearer insights into the benefits and possible practical applications, highlighting the importance and innovation of the present work.

We examined the performance parameters of SPR in the ultraviolet, visible, and near-infrared ranges at an operating wavelength of 300-1000 nm. It is clear from the results in Figure 2, that the SPR characteristic completely disappears at

small wavelengths, particularly at 300, 400, and 500 nm. Since the sensor layer absorbs the SPR wave energy, the reflectance at the Au/water interface is low across the whole angle range. The SPR wave appears at 600, 700, 900, 700, and 1000 nm wavelengths, and the resonance angle (Θ_{spr}) is 60°, 54.5°, 51.5°, and 50.5°, respectively. Tiny variations in the sensing layer's refractive index will result in a small shift in the SPR angle, which was achieved at 61.5°, 55.5°, 52.5°, and 51.5° for the same wavelengths.

The reflectivity curves show that there is no angular interrogation at the wavelengths of 300, 400, and 500 nm. The response appears at wavelengths of 600 and 700 nm and then disappears at 800 nm. Surface plasmon wave production completely disappears for all SnSe layer thicknesses, as water shows anomalous scattering [31]. The SPR angles decrease with increasing wavelengths, while they are constant at all thicknesses of the SnSe layer. The greater reflection intensity at 1000 nm when $d=0$ is 0.96 for ($\Delta n=0$ and $\Delta n=0.01$); this value reduces slightly at $d=80$ nm to reach 0.95 in the same conditions.

When surface plasmons are excited at longer wavelengths (and lower incidence angles), the reflection dips affected by

this excitation are narrower than when surface plasmons are excited at shorter wavelengths (and higher incidence angles). Figure 2 shows the lowest FWHM value at 600 nm was found at 9° with a thickness of 10, 20, 30, 40 nm for an analyte RI of 1.33. On the other hand, the FWHM value changed to 9.3° at (10, 20, 30)nm thickness as a result of a change in the analyte RI from 1.33 to 1.34, which is indicated in bold in Table 1. The FWHM value reaches 2.1° and 0.8° at wavelengths of 700 nm and 900 nm, respectively, which were indicated in bold in Tables 2 and 3, as the wavelength and layer thickness increase. Subsequently, it takes a minimum value of 0.7° at the 1000 nm wavelength (see Table 4). Due to the SnSe material's small bandgap and higher absorption efficiency, the SPR dip gets its maximum value of 0.95° at 900 nm.

A greater sensitivity of the biosensor can be achieved at the lowest FWHM value and the longest SPR dip. Actually, as the wavelengths changed, the SPR dip changed, and the FWHM value decreased, resulting in an increase in the detection accuracy. The biosensor's sensitivity values of 140deg/RIU and 110deg/RIU at 600 and 700 nm, respectively, were disregarded due to the low detection accuracy values as displayed in Tables 1 and 2 for all SnSe thicknesses. Consequently, the maximum sensitivity of an SPR instrument does not necessarily translate to the best sensitivity for detecting molecule binding, also known as surface sensitivity. As the wavelength increases, the SPR-created evanescent field's penetration length into the fluid medium grows. Although longer wavelengths can penetrate farther than the sensor surface, surface sensitivity is significantly lost in the process. The maximum sensitivity of the suggested biosensor is 100deg/RIU at wavelength 900 nm. For thicknesses of 0, 10, 70, and 80 nm, the sensitivity is 100deg/RIU at wavelength 1000 nm. As seen in Table 4, it obtained the greatest detection accuracy of 1.42.

From Tables 1-4, it is clear that there is a change in the calculated values of the parameters FWHM, DA, and QF. Where it is attributed that the parameters of the designed model have an effect on those parameters when the thickness of the SnSe layer is changed. In addition to the fact that reflectivity, transmittance, and absorbance vary with angle of incidence, this also depends on the change in refractive index values of the materials utilized as a function of wavelength; the absorption value is necessarily impacted by variations in thickness, and these changes have an impact on the computed values of these parameters. The depth and length of the prism can also have an effect on sensitivity.

6. CONCLUSIONS

The designed biosensor was simulated numerically based on the TMM calculation method, and the performance characteristics were verified. The biosensor that was designed is a modified surface plasmon resonance sensor that is based on the Otto configuration. The research involves adjusting the wavelength from 300 to 1000 nm and the thickness of the SnSe layer from 0 to 80 nm. The angle of incidence of the incoming beam was varied between 0° and 90°. The value of Δn for the external sensing media was assumed to be variable in order to detect the presence of contamination present in the medium; that is, if the value is zero, the medium is pure, and if it is (0.01), the medium is polluted, indicating that contamination has changed the refractive index of the medium.

The work focuses on determining the optimal incidence

angles where plasmonic resonance happens, which has not been accomplished in earlier investigations of this model. Our research seeks to give an appropriate design and numerical values for the parameters that might help improve the performance of biological sensors in practice. In order to make well-informed design decisions, we investigated the effect of several design parameters on sensor performance, such as SnSe and Au layer thickness, wavelength used, and the refractive index of the sensing medium. According to the findings, the designed SnSe/Au surface plasmon instrument unquestionably has a high sensitivity for detecting pollution—an essential feature for biosensor instruments.

The SPR wave appeared at 600, 700, 900, 700, and 1000 nm wavelengths, and the resonance angle (Θ_{spr}) is 60°, 54.5°, 51.5°, and 50.5°, respectively. While, at the same wavelengths, tiny variations in the sensing layer's refractive index will result in a small shift in the resonance angle (Θ_{spr}), which was achieved at 61.5°, 55.5°, 52.5°, and 51.5°, respectively.

It was found that the highest sensitivity measured was 140 degrees/RIU at a wavelength of 600 nm in thickness (0, 40, and 80 nm). This value was disregarded due to the low detection accuracy of 0.15, so the best sensitivity of the proposed biosensor was found at the wavelength of 900 nm, where the sensitivity reached 100 for all thicknesses. Similarly, at the wavelength of 1000 nm, the sensitivity reached 100 degree/RIU for thicknesses of (0, 10, 70, and 80 nm), with a DA, L_d , QF, and FWHM of 1.43, 0.93°, 143 RIU⁻¹, and 0.7°, respectively. All parameters were identified in the sensing medium and changed to ($\Delta n=0.01$). As a result, the designed biosensor can identify hard water and detect biological liquids dissolved in the water. Consequently, we recommend designing and constructing this model and applying it practically, taking into account the parameter values (the angles of incidence of the light source, refractive indices of the sensing medium, wavelength used, thickness of tin selenide layers) mainly in the configuration.

ACKNOWLEDGMENT

The authors would like to express their gratitude to Mustansiriya University (www.uomustansiriya.edu.iq) in Baghdad, Iraq, for its assistance with this work.

REFERENCES

- [1] Ravindran, N., Kumar, S., CA, M., Thirunavookarasu S, N., CK, S. (2023). Recent advances in Surface Plasmon Resonance (SPR) biosensors for food analysis: A review. *Critical Reviews in Food Science and Nutrition*, 63(8): 1055-1077. <https://doi.org/10.1080/10408398.2021.1958745>
- [2] Alzahrani, F.A., Sorathiya, V. (2023). Phase change material and MXene composited refractive index sensor for a wide range of sensing applications at visible and infrared wavelength spectrum. *Optik*, 272: 170242. <https://doi.org/10.1016/j.ijleo.2022.170242>
- [3] Lahav, A., Auslender, M., Abdulhalim, I. (2008). Sensitivity enhancement of guided-wave surface-plasmon resonance sensors. *Optics Letters*, 33(21): 2539-2541. <https://doi.org/10.1364/OL.33.002539>
- [4] Rahman, M.S., Anower, M.S., Abdulrazak, L.F. (2019). Modeling of a fiber optic SPR biosensor employing Tin

- Selenide (SnSe) allotropes. *Results in Physics*, 15: 102623. <https://doi.org/10.1016/j.rinp.2019.102623>
- [5] Mitsushio, M., Miyashita, K., Higo, M. (2006). Sensor properties and surface characterization of the metal-deposited SPR optical fiber sensors with Au, Ag, Cu, and Al. *Sensors and Actuators A: Physical*, 125(2): 296-303. <https://doi.org/10.1016/j.sna.2005.08.019>
- [6] Zhou, W., Qin, X., Lv, M., Qiu, L., Chen, Z., Zhang, F. (2023). Design of a new type of in-hole gold-coated high-performance quasi-PCF sensor enhanced with surface plasmon resonance. *Coatings*, 13(7): 1261. <https://doi.org/10.3390/coatings13071261>
- [7] Daniyal, W.M.E.M.M., Fen, Y.W., Fauzi, N.I.M., Hashim, H.S., Ramdzan, N.S.M., Omar, N.A.S. (2020). Recent advances in surface plasmon resonance optical sensors for potential application in environmental monitoring. *Sensors and Materials*, 32(12): 4191-4200. <https://doi.org/10.18494/SAM.2020.3204>
- [8] El-Chaghaby, G.A., Rashad, S. (2024). Nanosensors in Agriculture: Applications, prospects, and challenges. In *Handbook of Nanosensors: Materials and Technological Applications*, Springer, Cham, pp. 1303-1330. https://doi.org/10.1007/978-3-031-16338-8_52-1
- [9] Valenzuela-Amaro, H.M., Aguayo-Acosta, A., Meléndez-Sánchez, E.R., de la Rosa, O., Vázquez-Ortega, P.G., Oyervides-Muñoz, M.A., Sosa-Hernández, J.E., Parra-Saldívar, R. (2023). Emerging applications of nanobiosensors in pathogen detection in water and food. *Biosensors*, 13(10): 922. <https://doi.org/10.3390/bios13100922>
- [10] Janith, G.I., Herath, H.S., Hendeniya, N., Attygalle, D., Amarasinghe, D.A.S., Logeeshan, V., Wickramasinghe, P.M.T.B. Wijayasinghe, Y.S. (2023). Advances in surface plasmon resonance biosensors for medical diagnostics: An overview of recent developments and techniques. *Journal of Pharmaceutical and Biomedical Analysis Open*, 100019. <https://doi.org/10.1016/j.jpba.2023.100019>
- [11] Srivastava, S., Yadav, S., Mishra, A.C., Singh, S., Lohia, P., Dwivedi, D.K., Yadav, R.K., Hossain, M.K. (2024). Ultra-Sensitive surface plasmon resonance biosensor for liver metastases and hepatocellular carcinoma detection using silicon nitride and black phosphorus nanomaterial. *Plasmonics*, 19(2): 1031-1041. <https://doi.org/10.1007/s11468-023-02059-6>
- [12] Azab, M.Y., Hameed, M.F.O., Obayya, S.S. (2023). Overview of optical biosensors for early cancer detection: fundamentals, applications and future perspectives. *Biology*, 12(2): 232. <https://doi.org/10.3390/biology12020232>
- [13] Nylander, C., Liedberg, B., Lind, T. (1982). Gas detection by means of surface plasmon resonance. *Sensors and Actuators*, 3: 79-88. [https://doi.org/10.1016/0250-6874\(82\)80008-5](https://doi.org/10.1016/0250-6874(82)80008-5)
- [14] Dai, X., Liang, Y., Zhao, Y., Gan, S., Jia, Y., Xiang, Y. (2019). Sensitivity enhancement of a surface plasmon resonance with tin selenide (SnSe) allotropes. *Sensors*, 19(1): 173. <https://doi.org/10.3390/s19010173>
- [15] Dwivedi, A.K., Srivastava, A., Tripathi, S. (2022). Tin di-selenide and zinc oxide based SPR biosensor for detection of DNA hybridization, anemia and abnormality in urine. *Optical and Quantum Electronics*, 54(6): 366. <https://doi.org/10.1007/s11082-022-03759-9>
- [16] Varasteanu, P. (2021). Optimizing the tin selenide (SnSe) allotrope/gold-based surface plasmon resonance sensors for enhanced sensitivity. *Plasmonics*, 16(2): 341-347. <https://doi.org/10.1007/s11468-020-01255-y>
- [17] Mohamad, H.J., Kafi, S.H., Taban, D.A. (2023). Ag/CdS surface plasmon simulation systems for gas sensor. *Kuwait Journal of Science*, 50(3): 216-222. <https://doi.org/10.1016/j.kjs.2023.05.007>
- [18] Mohamad, H.J., Kafia, S.H., Kadhum, F.J. (2024). Surface plasmon resonance analysis for benzene sensing media using silver and Ta₂O₅ thin films. *Malaysian Journal of Science*, 96-103. <https://doi.org/10.22452/mjs.vol43no2.10>
- [19] Sun, Y., Cai, H., Wang, X., Zhan, S. (2019). Optimization methodology for structural multiparameter surface plasmon resonance sensors in different modulation modes based on particle swarm optimization. *Optics Communications*, 431: 142-150. <https://doi.org/10.1016/j.optcom.2018.09.027>
- [20] Lin, C., Chen, S. (2019). Design of highly sensitive guided-wave surface plasmon resonance biosensor with deep dip using genetic algorithm. *Optics Communications*, 445: 155-160. <https://doi.org/10.1016/j.optcom.2019.04.035>
- [21] Sebek, M., Thanh, N.T.K., Su, X., Teng, J. (2023). A genetic algorithm for universal optimization of ultrasensitive surface plasmon resonance sensors with 2D materials. *Acs Omega*, 8(23): 20792-20800. <https://doi.org/10.1021/acsomega.3c01387>
- [22] Amoosoltani, N., Zarifkar, A., Farmani, A. (2019). Particle swarm optimization and finite-difference time-domain (PSO/FDTD) algorithms for a surface plasmon resonance-based gas sensor. *Journal of Computational Electronics*, 18: 1354-1364. <https://doi.org/10.1007/s10825-019-01391-7>
- [23] Yue, C., Ding, Y., Tao, L., Zhou, S., Guo, Y. (2023). Differential evolution particle swarm optimization for phase-sensitivity enhancement of surface plasmon resonance gas sensor based on MXene and blue phosphorene/transition metal dichalcogenide hybrid structure. *Sensors*, 23(20): 8401. <https://doi.org/10.3390/s23208401>
- [24] Junfeng, D., Li-hui, F. (2023). Application of dynamic baseline adjustment based on swarm intelligence optimization in the signal processing of fiber SPR sensor. *Optik*, 273: 170470. <https://doi.org/10.1016/j.ijleo.2022.170470>
- [25] Rahman, M.M., Abdulrazak, L.F., Ahsan, M., Based, M.A., Rana, M.M., Anower, M.S., Haider, J., Gurusamy, S. (2021). 2D nanomaterial-based hybrid structured (Au-WSe 2-PtSe 2-BP) surface plasmon resonance (SPR) sensor with improved performance. *IEEE Access*, 10: 689-698. <https://doi.org/10.1109/ACCESS.2021.3137420>
- [26] Huang, T., Zeng, S., Zhao, X., Cheng, Z., Shum, P.P. (2018). Fano resonance enhanced surface plasmon resonance sensors operating in near-infrared. In *Photonics*. MDPI, 5(3): 23. <https://doi.org/10.3390/photonics5030023>
- [27] Kumar, S., Yadav, A., Malomed, B.A. (2023). High performance surface plasmon resonance based sensor using black phosphorus and magnesium oxide adhesion layer. *Frontiers in Materials*, 10: 1131412. <https://doi.org/10.3389/fmats.2023.1131412>
- [28] Kushwaha, A.S., Kumar, A., Kumar, R., Srivastava, S.K.

- (2018). A study of surface plasmon resonance (SPR) based biosensor with improved sensitivity. *Photonics and Nanostructures-Fundamentals and Applications*, 31: 99-106. <https://doi.org/10.1016/j.photonics.2018.06.003>
- [29] Singh, S., Sharma, A.K., Lohia, P., Dwivedi, D.K., Sadanand, Fouad, H., Akhtar, M.S. (2022). Sensitivity enhancement of SPR biosensor employing heterostructure blue phosphorus/MoS2 and silicon layer. *Emerging Materials Research*, 11(2): 239-250. <https://doi.org/10.1680/jemmr.22.00009>
- [30] Umar, A., Ibrahim, A.A., Kumar, R., Rana, K., Algadi, H., Alhamami, M.A., Elsddig, M.M.E., Mohammed, A.Y. (2021). Aluminum doped ZnO nanorods for enhanced phenylhydrazine chemical sensor applications. *Science of Advanced Materials*, 13(12): 2483-2488. <https://doi.org/10.1166/sam.2021.4168>
- [31] Hancer, M., Sperline, R.P., Miller, J.D. (2000). Anomalous dispersion effects in the IR-ATR spectroscopy of water. *Applied Spectroscopy*, 54(1): 138-143. <https://doi.org/10.1366/0003702001948222>

NOMENCLATURE

B tangential component of magnetic field

E tangential component of electric field
 n_o refractive index of the glass prism
 n_k refractive index of corresponding layers
 R reflectance intensity of p-polarized light
 r_p reflection coefficient
 Δn_s variation in refractive indices

Greek symbols

β_k phase thickness
 $\Delta\theta_{RES}$ change in resonance angle, degrees
 ϵ_k dielectric constant, $F.m^{-1}$
 θ_o angle of incidence, degrees
 λ wavelength of incident light, nm
 Ω characteristic matrix of multilayer structure

Subscripts

D Thickness, nm
 DA detection accuracy
 FWHM full-width half maximum, degree
 L_d SPR dip
 QF quality factor, RIU^{-1}
 RC reflectivity curve
 S Sensitivity, $deg. RIU^{-1}$